# Chemical and thermal freeze-out parameters from 1*A* to 200*A* GeV

J. Cleymans*
*Department of Physics, University of Cape Town, Rondebosch 7701, South Africa*

K. Redlich
*Gesellschaft für Schwerionenforschung, D-64291 Darmstadt, Germany*
*and Institute for Theoretical Physics, University of Wrocław, PL-50204 Wrocław, Poland*
(Received 29 March 1999; published 19 October 1999)

The present knowledge about hadrons produced in relativistic heavy ion collisions is compatible with chemical freeze-out happening when the energy density divided by the particle density reaches the value of 1 GeV. This observation is used to determine the energy dependence of the chemical freeze-out parameters $T_{ch}$ and $\mu_B^{ch}$ for beam energies varying between 1 and 200*A* GeV. The consequences of this energy dependence are studied for various particle ratios. Predictions for particle ratios at beam energy 40*A* GeV are presented. The conditions for thermal freeze-out are also determined. These correspond either to an energy density of 45 MeV/fm$^3$ or to a particle density of 0.05/fm$^3$. [S0556-2813(99)03911-4]

PACS number(s): 25.75.Dw, 12.38.Mh, 24.10.Nz, 25.75.Gz

## I. INTRODUCTION

It is the purpose of the present paper to determine the energy dependence of the chemical freeze-out parameters, namely, the temperature $T_{ch}$ and the baryon chemical potential $\mu_B^{ch}$ for beam energies in the range between 1 and 200*A* GeV [1]. This covers the full range of energies available at the GSI Schwerionensynchrotron (SIS), BNL Alternating Gradient Synchrotron (AGS) and the CERN Super Proton Synchrotron (SPS) experiments. These parameters determine the particle composition of the hadronic final state. Below this temperature inelastic collisions between hadrons are no longer important and the hadronic abundances remain unchanged. This information can then be used to make predictions for beam energies that are in between those of the above experiments and also, eventually, to extrapolate results to higher beam energies.

To determine in a relatively unambiguous way the chemical freeze-out values in relativistic heavy ion collisions it is best to use ratios of integrated particle yields. Such ratios are not very sensitive to the dynamics of the underlying processes, one of the reasons being that integrated particle yields are Lorentz invariant, i.e., a boost in the transverse direction affects the momentum distribution of particles but not their number. The restriction to integrated particle yields therefore minimizes the model dependence of the freeze-out parameters. This of course is not true for particle yields restricted to narrow kinematic regions since these will be more dependent on the dynamics of the process. During the past few years such analyses have been made for the CERN SPS [2–9], the BNL AGS [10–13] and the GSI SIS [14,15] data. A discussion and review of the various results can be found in Ref. [16].

The momentum distribution of particles produced in relativistic heavy ion collisions does not show the dependence predicted by a statistical distribution. The longitudinal direction bears no resemblance to an exponential, and in the transverse direction substantial deviations from an exponential fit with a universal slope corresponding to the temperature exist.

In Sec. II we discuss the general case of hydrodynamic flow starting from the Cooper-Frye formula [17]. As a particular case we consider boost invariant longitudinal flow [18] accompanied by flow in the transverse direction. We next discuss the case where the longitudinal flow is reproduced by a superposition of fireballs. In all these cases particle ratios can be calculated as if they were given by a static Boltzmann distribution.

In Sec. III we discuss the exact conservation of strangeness in statistical models. This is necessary when the number of strange particles is very small as is the case in, e.g., the GSI SIS energy range.

In Sec. IV we use the phenomenological observation that the freeze-out parameters all correspond to an average energy per hadron of 1 GeV, independent of the manner in which the system was created, to extract the energy dependence of $T_{ch}$ and $\mu_B^{ch}$. This dependence is then used to track the behavior of various hadronic ratios as a function of energy and to present predictions for a beam energy of 40 GeV. We also determine the conditions for thermal freeze-out in the energy range between 1*A* GeV and 200*A* GeV. The values obtained previously [19–27] are compatible with an energy density $\epsilon \approx 45$ MeV/fm$^3$ or a particle density $n \approx 0.05$ fm$^{-3}$. It is at present not possible to distinguish between these two possibilities.

In Sec. V we summarize our results.

## II. RATIOS OF THERMAL PARTICLE ABUNDANCES

In the thermal model particle densities are determined by a statistical distribution, denoted $n_i^0$ where the index $i$ refers to the type of hadron, e.g., $i=\pi^+, K^+, \ldots$ etc. In the Boltzmann approximation $n_i^0$ is given by

$$n_i^0 = g \int \frac{d^3p}{(2\pi)^3} e^{-(E_i-\mu_i)/T} = \frac{g m_i^2 T}{2\pi^2} K_2(m_i/T) e^{\mu_i/T}. \tag{2.1}$$

*On sabbatical leave at the Fakultät für Physik, Universität Bielefeld, D-33615 Bielefeld, Germany.

 

This expression applies for the density of particles inside a fireball at rest having a temperature $T$ and particle $i$ having a chemical potential $\mu_i$. If the system is in chemical equilibrium then the possible values of $\mu_i$ are determined by the overall baryon chemical potentials for baryon number $\mu_B$, strangeness $\mu_S$, and charge $\mu_Q$. The value of $\mu_B$ is fixed by giving the overall baryon number density $n_B$, and that of $\mu_S$ by fixing the overall strangeness to zero, the value of $\mu_Q$ is fixed by giving the neutron surplus. If the number of initial state neutrons is equal to the number of protons as is the case in, e.g., S-S then $\mu_Q=0$, for Pb-Pb $\mu_Q$ is small and negative. This means that for given values of $T$ and $\mu_B$ one tunes the remaining parameters, $\mu_S$ and $\mu_Q$, in such a way as to ensure strangeness neutrality and the correct isospin composition of the system.

At chemical freeze-out the particle density of hadrons of a given type is determined by summing over all hadronic densities multiplied by the appropriate branching ratio, e.g., for $\pi^+$ one has

$$n_{\pi^+}=\sum_i n_i B(i\to\pi^+). \tag{2.2}$$

We have included in Eq. (2.2) the contributions from all particles and resonances with masses up to 2 GeV [28]. Thermal freeze-out happens when the elastic collisions between hadrons cease. Since it is obvious that the Boltzmann distribution is not a good description of the momentum distribution of particles in relativistic heavy ion collisions we will now discuss modifications which lead to a more realistic description of the particle spectra.

### A. Cooper-Frye formula

In a hydrodynamic description taking into account flow in the longitudinal and transverse directions, the final state particles will leave the hadronic gas at freeze-out time. The momentum distribution of particles is given by the Cooper-Frye formula [17]

$$E\frac{dN}{d^3p}=\frac{g}{(2\pi)^3}\int_\sigma f(x,p)p^\mu d\sigma_\mu, \tag{2.3}$$

where the integration has to be performed over the freeze-out surface described by $\sigma_\mu$. Its direction is perpendicular to the surface and its magnitude is determined by the size of the freeze-out surface. For the temperatures under consideration it is safe to neglect quantum statistics and we will therefore work with the Boltzmann distribution from now on; the generalization to Fermi-Dirac or Bose-Einstein statistics is straightforward. We thus have

$$f(x,p)=\exp[(-p\cdot u+\mu)/T], \tag{2.4}$$

where $T$, $\mu$, and $u^\mu$ are the (space-time dependent) temperature, chemical potential, and four-velocity, respectively [29]. As an example, for a static fireball, the freeze-out surface is given by

$$d\sigma^\mu=(d^3x,\vec{0}), \tag{2.5}$$

so that we obtain the expected result

$$E\frac{dN}{d^3p}=\frac{gV}{(2\pi)^3}E\exp[(-E+\mu)/T]. \tag{2.6}$$

After integrating the differential distribution over all momenta one obtains the total number of particles [1,30]

$$\begin{aligned}N&=\frac{g}{(2\pi)^3}\int\frac{d^3p}{E}\int_\sigma f(x,p)p^\mu d\sigma_\mu\\&=\frac{g}{(2\pi)^3}\int_\sigma d\sigma_\mu\int\frac{d^3p}{E}f(x,p)p^\mu.\end{aligned} \tag{2.7}$$

For a Boltzmann distribution this becomes

$$N=\frac{g}{(2\pi)^3}\int_\sigma d\sigma_\mu u^\mu\left[4\pi Tm^2K_2\left(\frac{m}{T}\right)\right]. \tag{2.8}$$

As a consequence,

$$\frac{N_i}{N_j}=\frac{n_i^0}{n_j^0}. \tag{2.9}$$

Thus effects of hydrodynamic flow cancel out in the hadronic ratio, provided there are unique freeze-out temperature and chemical potential.

### B. Rapidity plateau and transverse expansion

For boost-invariant cylindrical expansion along the $z$ axis the correct variable to use is the proper time $\tau$ (recall $d^4x=\tau d\tau dy r dr d\phi$). We have

$$d\sigma^\mu=(\tau dy r dr d\phi,\hat{r}\tau d\tau dy r d\phi), \tag{2.10}$$

where the second component is in the $\hat{r}$ direction, i.e., perpendicular to the surface of the cylinder. For the case where the flow is azimuthally symmetric, i.e., when an average is made over all events or when only head-on collisions are considered, one has therefore [31,32]

$$\begin{aligned}&\left(\frac{dN_i}{dy m_t dm_t}\right)_{y=0}\\&=\frac{g}{\pi}\int_\sigma r dr\tau_F(r)\left\{m_tI_0\left(\frac{p_t\sinh y_t}{T_{ch}}\right)K_1\left(\frac{m_t\cosh y_t}{T_{ch}}\right)\right.\\&\left.-\left(\frac{\partial\tau_F}{\partial r}\right)p_tI_1\left(\frac{p_t\sinh y_t}{T_{ch}}\right)K_0\left(\frac{p_t\cosh y_t}{T_{ch}}\right)\right\}e^{\mu_i/T_{ch}},\end{aligned} \tag{2.11}$$

where $\tau_F(r)$ refers to the freeze-out time which in general depends on $r$, so that the center of the cylinder freezes out before the surface.

After integration over the transverse mass $m_T$ this leads to

$$\left(\frac{dN_i}{dy}\right)_{y=0} = \frac{g}{\pi}\int_\sigma r\,dr\,\tau_F(r)\left\{\cosh(y_T) - \left(\frac{\partial \tau_F}{\partial r}\right)\sinh(y_T)\right\} m_i^2 T_{ch} K_2\left(\frac{m_i}{T_{ch}}\right) e^{\mu_i/T_{ch}}. \tag{2.12}$$

If the freeze-out temperature is the same everywhere on the freeze-out surface this leads to the surprisingly simple result that the ratios are unaffected by the hydrodynamic flow:

$$\frac{(dN_i/dy)_{y=0}}{(dN_j/dy)_{y=0}} = \frac{m_i^2 T_{ch} K_2\left(\frac{m_i}{T_{ch}}\right) e^{\mu_i/T_{ch}}}{m_j^2 T_{ch} K_2\left(\frac{m_j}{T_{ch}}\right) e^{\mu_j/T_{ch}}} = \frac{n_i^0}{n_j^0}. \tag{2.13}$$

This is a case where the momentum distribution in no way resembles a Boltzmann distribution: the rapidity distribution is flat and the transverse momentum distribution is affected by transverse flow, yet the integrated ratios are the same as those of a static Boltzmann distribution.

### C. Superposition of fireballs

In order to reproduce more closely the observed rapidity distribution it is useful to consider a superposition of fireballs along the rapidity axis [33]. The resulting particle density (integrated over the particle rapidity $y$) is given by

$$n_i = \int_{-\infty}^{\infty} dy \int_{-Y}^{Y} dY_{FB}\,\rho(Y_{FB})\frac{dn_i^0}{dy}(y - Y_{FB}), \tag{2.14}$$

where $Y_{FB}$ is the position of the fireball, $\rho$ is the distribution of fireballs, and $Y$ is the largest value of the position in rapidity space of a fireball. In the above integral it is possible to interchange the integration limits so that one obtains

$$n_i = n_i^0 \int_{-Y}^{Y} dY_{FB}\,\rho(Y_{FB}). \tag{2.15}$$

In a ratio the integral over the distribution of fireballs cancels out so that one is left with

$$\frac{n_i}{n_j} = \frac{n_i^0}{n_j^0}, \tag{2.16}$$

with the conclusion that the ratio is the same as if it were given by a Boltzmann distribution. Note that the cancellation is only possible if all fireballs are of a similar nature, i.e., they all have the same temperature.

## III. EXACT STRANGENESS CONSERVATION

In relativistic heavy ion collisions the energy and the number of hadrons in the final state is large enough to justify the use of the grand canonical ensemble. However if the temperature is very low, as is the case for the data from GSI SIS, then the number of strange particles in the final state is very small and it becomes necessary to take this into account by using exact strangeness conservation [34–41]. The grand canonical ensemble only enforces strangeness conservation on average and allows for fluctuations around strangeness zero. This is not good enough if the number of strange particles is very small. The same holds for applications of statistical descriptions to a small system like the ones created in $p-p$ or $e^+-e^-$ collisions as has been done recently in Ref. [42].

We therefore treat strangeness exactly, especially in the GSI SIS energy range but continue to use a grand canonical description for baryon number and for charge since the number of baryons and charged particles is always large.

To restrict the ensemble summation to a fixed value of the strangeness $S$, one performs the following projection:

$$Z_S = \frac{1}{2\pi}\int_0^{2\pi} d\phi\;\; e^{-iS\phi} Z(T,\lambda_B,\lambda_S,\lambda_Q), \tag{3.1}$$

where the fugacity factor $\lambda_S$ has been replaced by

$$\lambda_S = e^{i\phi}, \tag{3.2}$$

and $Z$ is the standard grand canonical partition function. Neglecting for the moment the contribution of multistrange particles like $\Xi$'s and $\Omega$'s one can write the partition function as

$$Z_{S=0} = \frac{1}{2\pi}\int_0^{2\pi} d\phi \exp\{N_0 + N_1 e^{i\phi} + N_{-1} e^{-i\phi}\}, \tag{3.3}$$

here $N_1$ stands for the sum of all single particle partition functions with strangeness plus one:

$$N_{-1} \equiv N_\Lambda + N_{\bar{K}} + \cdots, \tag{3.4}$$

while $N_{-1}$ stands for the sum of all single particle partition functions with strangeness minus one:

$$N_1 \equiv N_{\bar{\Lambda}} + N_K + \cdots. \tag{3.5}$$

As an illustration we quote the explicit form of $N_\Lambda$ assuming Boltzmann statistics

$$N_\Lambda \equiv \frac{2V}{(2\pi)^3}\int d^3p \exp((-E_\Lambda + \mu_B)/T). \tag{3.6}$$

It is clear from the above equation that baryon number is being treated grand canonically.

To calculate the partition function more explicitly we expand each term in a power series:

$$Z_{S=0} = Z_0 \frac{1}{2\pi}\int_0^{2\pi} d\phi \sum_{m=0}^{\infty}\sum_{n=0}^{\infty}\frac{1}{m!}\frac{1}{n!} \times N_1^m N_{-1}^n \exp(im\phi)\exp(-in\phi), \tag{3.7}$$

where $Z_0$ is the standard partition function for all particles having zero strangeness. Performing the integration over $\phi$ we are left with

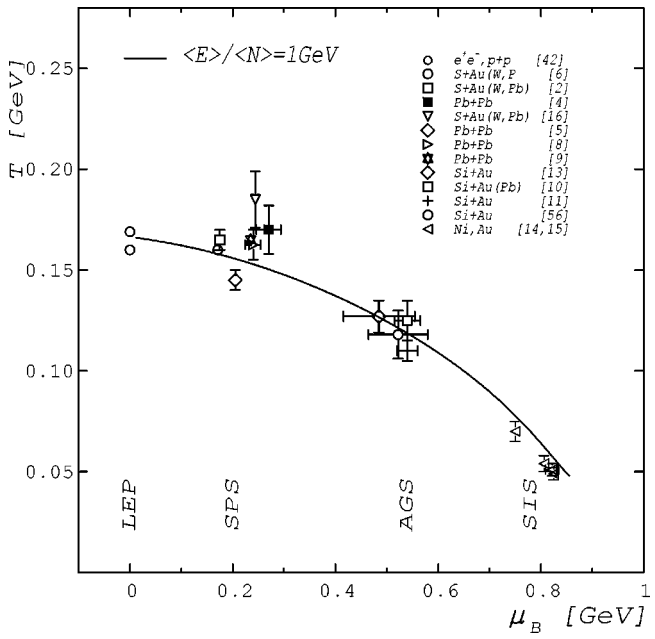


FIG. 1. Chemical freeze-out parameters $T_{ch}$ and $\mu_B^{ch}$ obtained at LEP, CERN SPS, BNL AGS, and GSI SIS. References to the points are given in Table I. The full line corresponds to an energy density over total particle density of 1 GeV.

$$Z_{S=0}=Z_0\sum_{n=0}^{\infty}\frac{1}{n!^2}(N_1N_{-1})^n, \tag{3.8}$$

where one recognizes the series expansion of the modified Bessel function

$$Z_{S=0}=Z_0I_0(x_1), \tag{3.9}$$

where $x_1\equiv 2\sqrt{N_1N_{-1}}$. The particle densities can be deduced in the standard way from the partition function. As an example we quote the number of kaons:

$$N_K=Z_K\frac{N_1}{\sqrt{N_1N_{-1}}}\frac{I_1(x_1)}{I_0(x_1)}. \tag{3.10}$$

The total energy density can be calculated from

$$\langle E\rangle=T^2\frac{\partial}{\partial T}\ln Z_{S=0}\Big|_{\lambda_i=1}. \tag{3.11}$$

Similarly, the particle number is given by

$$\langle N\rangle=T\frac{\partial}{\partial \mu_i}\ln Z_{S=0}\Big|_{\lambda_i=1}. \tag{3.12}$$

Of special interest is the small volume limit (or, more correctly, the small particle number limit). In this case the partition function can be expanded in a power series in which case the integration over $\phi$ gives zero for all cases where the oscillating factors do not match, i.e.,

TABLE I. Chemical freeze-out temperature $T_{ch}$ and baryon chemical potential $\mu_B^{ch}$ in various collisions.

| Energy | $T_{ch}$ [MeV] | $\mu_B^{ch}$ [MeV] | Reference |
|---|---|---|---|
| SPS | | | |
| Pb + Pb 158*A* GeV | 170±11 | 270±24 | [4] |
| Pb + Pb 158*A* GeV | 165 | 235 | [9] |
| Pb + Pb 158*A* GeV | 145±5 | 205±5 | [5] |
| S + S 200*A* GeV | 180.5±10.9 | 220.2±18.0 | [7] |
| S + Ag 200*A* GeV | 178.9±8.1 | 241.5±14.5 | [7] |
| S + S 200*A* GeV | 171.0 | 160.04 | [6] |
| S + S 200*A* GeV | 160.2±3.5 | 158.0±4.0 | [16] |
| S + S 200*A* GeV | 165.0±5.0 | 175.0±5.0 | [2] |
| AGS | | | |
| Si + Au 14.6*A* GeV | 127±8 | 485±70 | [13] |
| Si + Au 14.6*A* GeV | 130±10 | 540±20 | [10] |
| Si + Au 14.6*A* GeV | 118±12 | 522±58 | [56] |
| Si + Au 14.6*A* GeV | 110±5 | 540±20 | [11] |
| SIS | | | |
| Ni-Ni 1.9*A* GeV | 70±10 | 720±50 | [14,15] |
| Ni-Ni 0.8*A* GeV | 48±10 | 820±10 | [15] |
| Au-Au 1.0*A* GeV | 49±3 | 825±8 | [15] |
| Ni-Ni 1.0*A* GeV | 51±5 | 822±10 | [15] |
| Ni-Ni 1.8*A* GeV | 54±3 | 806±8 | [15] |

$$Z_{S=0}\approx 1+\frac{1}{2\pi}\int_0^{2\pi}d\phi\left[gV\int\frac{d^3p}{(2\pi)^3}e^{-E/T+i\phi}\right]\times\left[gV\int\frac{d^3p}{(2\pi)^3}e^{-E/T-i\phi}\right]+\cdots. \tag{3.13}$$

Thus it is clear that one needs at least two terms before one gets a nonvanishing result. For small particle numbers this leads to the well-known suppression of strangeness.

## IV. CHEMICAL AND THERMAL FREEZE-OUT PARAMETERS

### A. Chemical freeze-out

The considerations presented in the previous two sections make it possible to extract in a reliable way the values of the chemical freeze-out parameters $T_{ch}$ and $\mu_B^{ch}$ from ratios of integrated particle yields. This procedure has been followed repeatedly over the past few years and results obtained from CERN SPS, BNL AGS, and GSI SIS data are shown in Fig. 1, and in Table I we also show the results obtained in Ref. [42] from $e^+-e^-$ and $p-p$ collisions. A low energy beam creates a hadronic gas with a corresponding low value of $T_{ch}$ but a high value of the baryon chemical potential. This reflects the fact that such a system is predominantly made up of nucleons and contains relatively few mesons. At the other end, the CERN SPS beam creates a hadronic system which has a high $T_{ch}$ but a very low value of $\mu_B^{ch}$. This is because the hadronic system created is very rich in mesons and the proportion of baryons diminishes accordingly. It has been

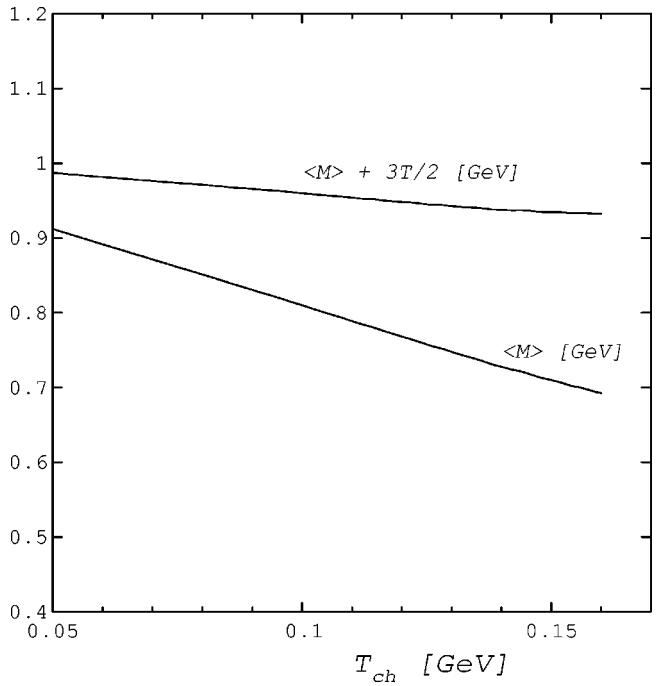


FIG. 2. Average mass along the freeze-out curve of Fig. 1 as a function of the chemical freeze-out temperature.

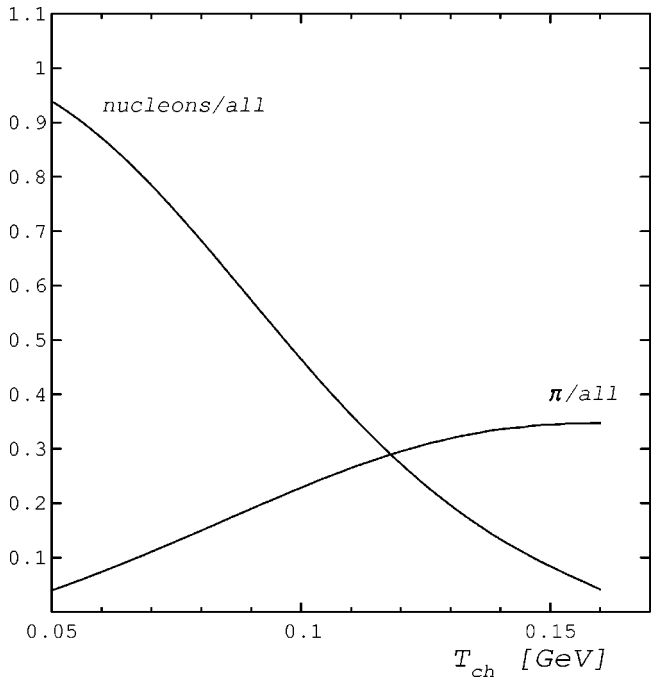


FIG. 3. Change of the particle composition of the hadronic gas along the freeze-out curve of Fig. 1 as a function of the chemical freeze-out temperature. Shown are the fractions of nucleons and of pions.

noted in Ref. [44] that, despite the wide variation in beam energies, all these points have in common the fact that the energy density divided by the total particle density is 1 GeV, independently of whether the system was created in Ni-Ni at 1*A* GeV or in S-S at 200*A* GeV. The energy density has been calculated using Eq. (3.11) and the particle density was calculated using Eq. (3.12). This means that, independently of how the system was created from the moment the average energy per hadron becomes less than 1 GeV, inelastic collisions cease to be important and the chemical composition of the final hadronic state is fixed. We consider this to be extremely remarkable.

Since the beam energy is increased smoothly as one follows the universal freeze-out curve, Fig. 1, it is possible to determine the energy dependence of the chemical freeze-out parameters, $T_{ch}$ and $\mu_B^{ch}$; this will be done explicitly in the next section. We first discuss some of the implications of the freeze-out curve.

### B. Nonrelativistic nature of hadronic gas

The phenomenological observation that the chemical freeze-out always corresponds to an average energy per hadron of 1 GeV per hadron is easy to understand in the GSI SIS energy range. Since the low temperature makes the hadronic gas a nonrelativistic one, nucleons dominate and only very few other particles are present, one can therfore use the approximation

$$\frac{\langle E\rangle}{\langle N\rangle}\approx m_N+\frac{3}{2}T\approx 1 \ \ \text{GeV}, \tag{4.1}$$

which immediately reproduces the value of 1 GeV per hadron.

At higher energies the hadronic gas becomes more and more mesonic in nature and pions and $\rho$ mesons dominate. It is of interest to compute the average mass of particles that make up the gas. This mass decreases very slowly, starting from the nucleon mass to approximately the $\rho$-meson mass. It is shown explicitly in Fig. 2. All hadrons in the gas are thus to a good approximation nonrelativistic, except for pions which dominate for low values of the baryon chemical potential. The nonrelativistic character is further enhanced by looking at the value of the average energy along the freeze-out curve; this is shown in Fig. 2. Thus the following relation holds:

$$\frac{\langle E\rangle}{\langle N\rangle}\approx\langle M\rangle+\frac{3}{2}T\approx 1 \ \ \text{GeV}. \tag{4.2}$$

The particle composition of the hadronic gas changes smoothly as one follows the universal freeze-out curve from low to high temperatures. At low temperatures the hadronic gas is dominated by nucleons, as can be seen explicitly in Fig. 3. For high temperatures the hadronic gas is meson dominated, with pions and rho mesons making up the largest fraction.

### C. Thermal freeze-out parameters

After chemical freeze-out, the particle composition inside the hadronic gas is fixed but elastic collisions still keep the system together until the final, thermal freeze-out. At this stage the momentum distribution of particles no longer changes and is then final. The transverse momentum spectra therefore determine the thermal freeze-out parameters. This

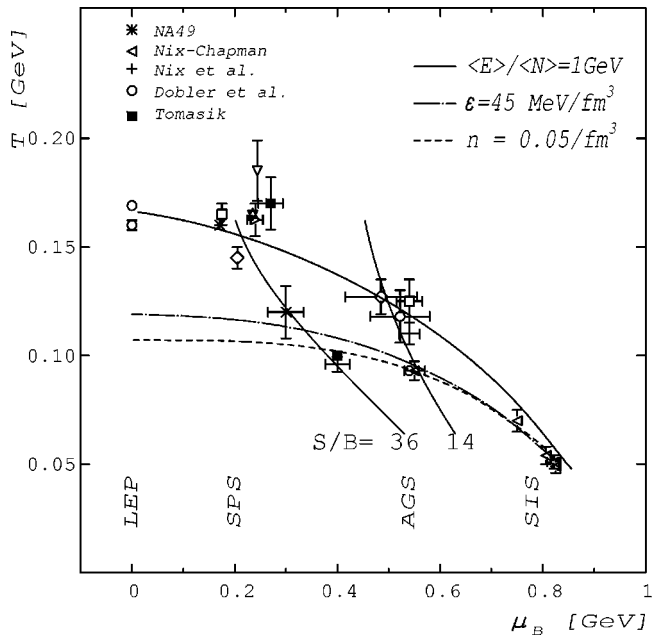


FIG. 4. Thermal freeze-out (dashed and dashed-dotted lines) and chemical freeze-out (solid line) curves. The dotted lines connecting the chemical and thermal freeze-out curves correspond to a fixed $S/B$ (entropy/baryon number) ratio. Only references to the thermal freeze-out points are indicated explicitly. See Fig. 1 for references to the chemical freeze-out points.

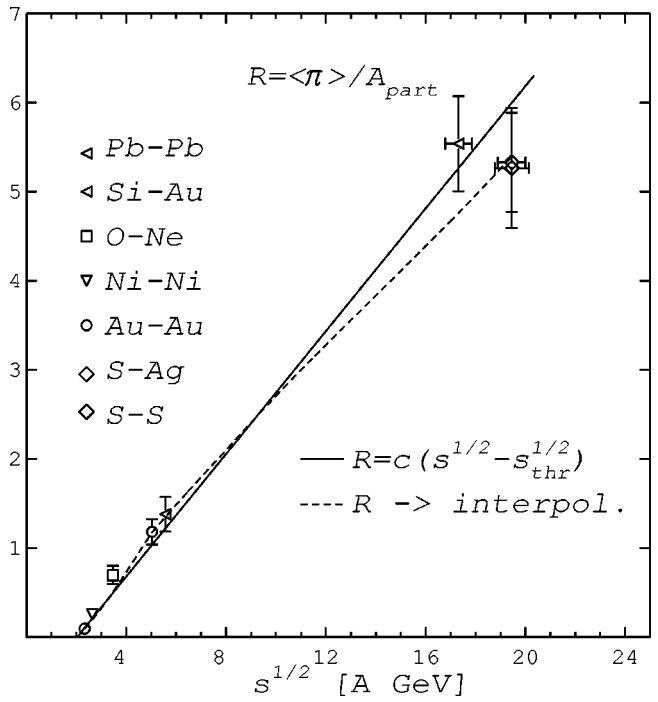


FIG. 5. Average number of pions divided by the number of participating nucleons as a function of the beam energy. The full line corresponds to a linear fit; the dashed line is a polynomial interpolation.

has been done by several groups in the past few years [19–27] and results are shown in Fig. 4. We have to remember that systematic errors on the particle spectra can be substantial and this introduces an additional uncertainty on the values of the parameters. The baryon chemical potential at this stage cannot be determined directly. We assume that the transition from chemical freeze-out to thermal freeze-out proceeds in such a way that the entropy to baryon number remains conserved, i.e., $S/B$ = constant. These are indicated by dashed-dotted lines in Fig. 4. We note that all results from 1$A$ GeV to 200$A$ GeV correspond to a fixed energy density of 45 MeV/fm$^3$, i.e., if the energy density inside the hadronic gas drops below this value, then the system ceases to exist independently of how it was formed. We note that it is not possible at present to distinguish between a fixed energy density and a fixed particle density. Both curves are shown in Fig. 4. The thermal freeze-out parameters are listed in Table II.

## V. DISCUSSION

### A. Energy dependence of chemical freeze-out parameters

An inspection of Fig. 1 suggests several possibilities for extracting the dependence of the thermal parameters on the beam energy. It would, e.g., be possible to plot the values of $T_{ch}$ as a function of the beam energy and simply interpolate between them. We follow a less direct method which relies on the use of results contained in Fig. 5. The values shown in this figure have been taken from the work of Gazdźicki [45,46] which uses a compilation of experimental results on the pion multiplicity divided by the number of spectator nucleons, $\langle\pi\rangle/A_{part}$. As can be seen from Fig. 5, in the relevant energy region this ratio increases approximately linearly with the beam energy or, more precisely with the variable

$$\sqrt{s}-\sqrt{s_{thr}}, \tag{5.1}$$

where $s_{thr}$ is the threshold energy for pion production given by

$$s_{thr}\equiv 2m_N+m_\pi. \tag{5.2}$$

This approximate linear dependence provides a convenient parametrization for extracting the energy dependence. A polynomial interpolation was also used in order to test the sensitivity of the parametrization. To extract the dependence on beam energy we combine Fig. 1 and Fig. 5. This is shown for one particular value in Fig. 6 where the crossing point between the two curves determines the value of the chemical freeze-out parameters. The resulting energy dependence of the freeze-out temperature $T_{ch}$ is shown in Fig. 7. As one can see, the value at first increases rapidly with beam energy and then converges towards a maximum value of approximately 160 MeV. We note that this value is very close to the expected phase transition to a quark-gluon plasma as indicated by results from lattice gauge theory which give an upper limit of about 170 MeV for the critical temperature [47]. The energy dependence of the baryon chemical potential is shown in Fig. 8. In this case the value at first decreases rapidly and then tends towards zero as the beam energy is increased.

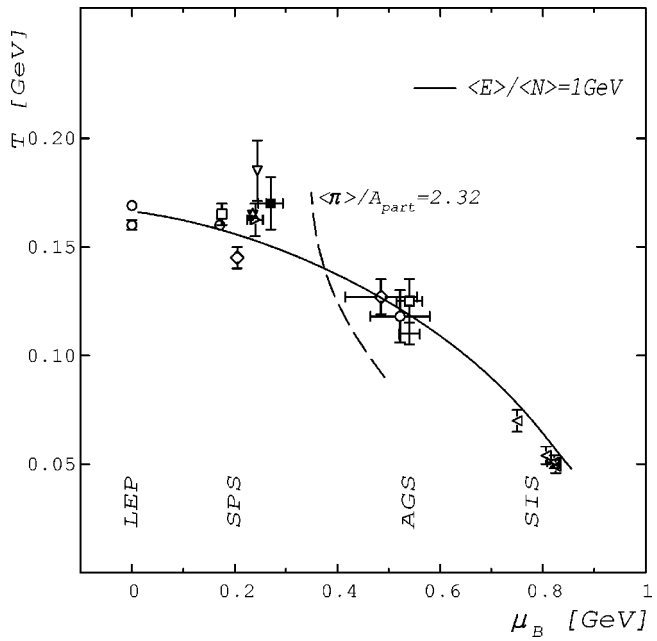


FIG. 6. Intersection between the chemical freeze-out curve and the line corresponding to a given ratio of pions to $A_{part}$. The intersection determines the values of $T_{ch}$ and $\mu_B^{ch}$ for the beam energy corresponding to the indicated $\pi/A_{part}$ ratio. References to the chemical freeze-out points are given in Fig. 1.

### B. Hadronic ratios

The energy dependence obtained for $T_{ch}$ and $\mu_B^{ch}$ in the previous subsection can be used to track various particle ratios as the beam energy increases. Of particular interest are the ratios of strange to nonstrange particles since it is widely believed that these show the largest deviation from chemical equilibrium. Several analyses have indicated the need for an additional parameter, $\gamma_S$, which measures the deviation from chemical equilibrium of strange hadrons [16,48]. The $K^+/\pi^+$ ratio is shown in Fig. 9—it increases smoothly from the low to the higher energies and reaches a maximum value of about 0.2 and stays approximately constant beyond this. We would like to refer to these values as the thermal model

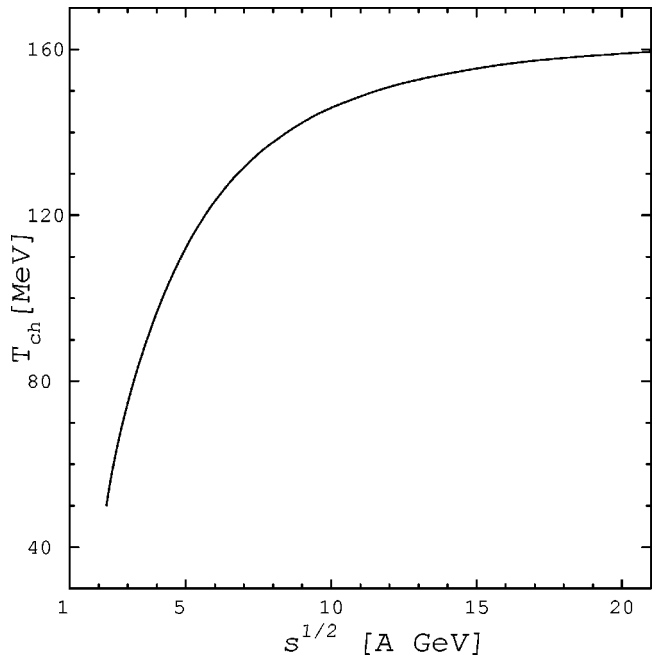


FIG. 7. Variation of the temperature at chemical freeze-out as a function of the beam energy.

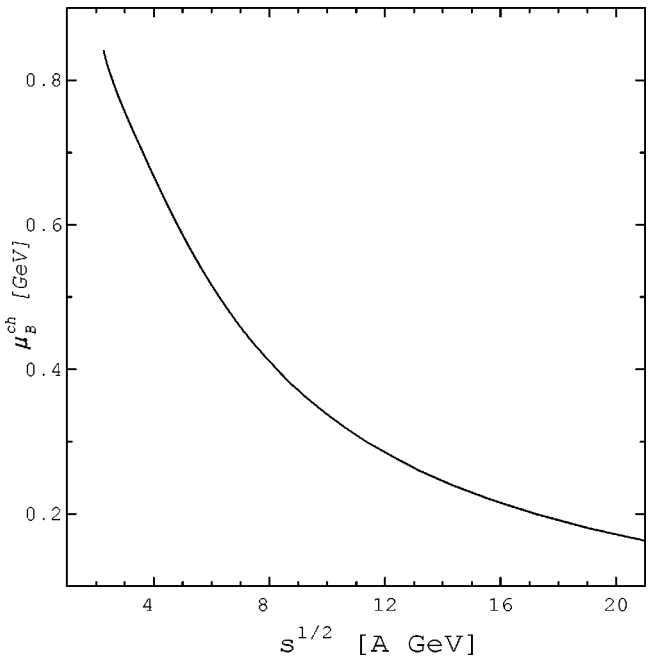


FIG. 8. Variation of the baryon chemical potential at chemical freeze-out as a function of the beam energy.

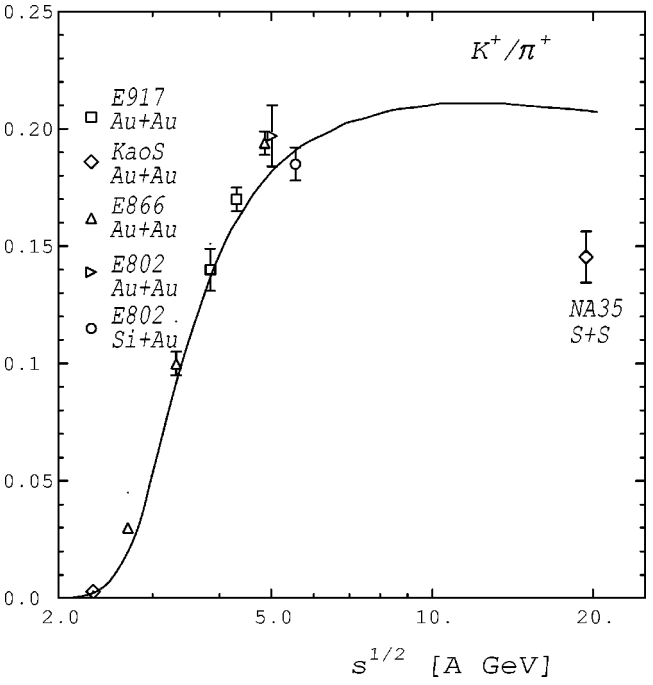


FIG. 9. Dependence of the $K^+/\pi^+$ ratio on beam energy along the chemical freeze-out curve of Fig. 1. Experimental results are indicated. See discussion in text.

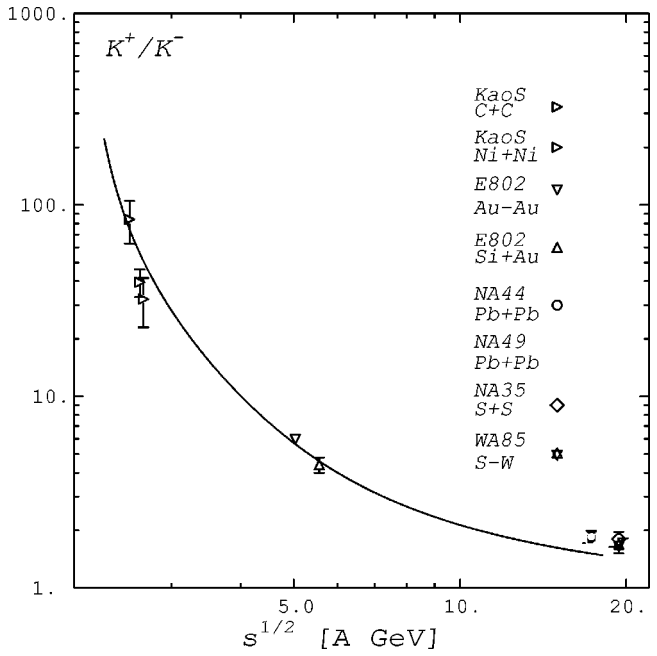


FIG. 10. Dependence of $K^+/K^-$ ratio on beam energy along the freeze-out curve of Fig. 1. Experimental results are indicated.

values for the $K^+/\pi^+$ ratio. Comparing these results with the experimental ones we see that the thermal values nicely track the observed ratio in the GSI and BNL energy range. Additional values of the $K^+/\pi^+$ ratio measured at midrapidity have become available recently from BNL AGS in the range 2–10.7*A* GeV [54]. All reported values are in good agreement with the thermal model values. However the CERN SPS value measured in S-S collisions is clearly below the predicted one. It has been argued recently [49–51] that this deviation is due to the formation of a quark-gluon plasma in the initial state of the relativistic heavy ion collision.

Next we consider the $K^+/K^-$ ratio. This ratio is extremely sensitive to the beam energy because it varies by two orders of magnitude over the energy range under consideration and is therefore a test of the thermal model. It is however not sensitive to the presence of $\gamma_S$ since it cancels out in the ratio. The comparison is shown in Fig. 10 and the agreement is good everywhere [55].

TABLE II. Thermal freeze-out temperature $T_f$ and baryon chemical potential $\mu_B^f$ in various collisions.

| Energy | $T_f$ [MeV] | $\mu_B^f$ [MeV] | Reference |
|---|---|---|---|
| SPS | | | |
| Pb + Pb 158*A* GeV | 120±12 | 300±35 | [19] [a] |
| Pb + Pb 158*A* GeV | 95.8±3.5 | 400±24 | [21] [a] |
| Pb + Pb 158*A* GeV | 100 | 400 | [53] |
| AGS | | | |
| Si + Au 14.6*A* GeV | 93.4±4.4 | 554±35 | [20] |
| Si + Au 14.6*A* GeV | 93 | 540 | [52] |

[a]The value of $\mu_b^f$ was estimated using isentropic expansion starting from the chemical freeze-out points.

TABLE III. Model predictions for $T=140$ MeV, $\mu_B=380$ MeV corresponding to beam energy of 40 GeV compared to experimental results obtained at 158 GeV.

| | Thermal model 40 GeV | Expt. data 158 GeV | Reference |
|---|---|---|---|
| $(p-\bar{p})/h^-$ | 0.382 | 0.228±0.029 | [19] |
| $\bar{p}/p$ | 0.006 | 0.055±0.010 | [8] |
| $\Lambda/K_s^0$ | 0.66 | 0.65±0.11 | [19] |
| $K^+/K^-$ | 2.34 | 1.85±0.09 | [8] |
| $\bar{\Lambda}/\Lambda$ | 0.014 | 0.128±0.012 | [43] |
| $\Xi^-/\Lambda$ | 0.12 | 0.127±0.011 | [43] |
| $\bar{\Xi}^-/\bar{\Lambda}$ | 0.24 | 0.180±0.039 | [43] |
| $\Xi^+/\Xi^-$ | 0.038 | 0.227±0.033 | [43] |
| $\bar{\Omega}^-/\Omega^-$ | 0.14 | 0.46±0.15 | [43] |

### C. Predictions

The results presented in the previous sections substantially increase the predictive power of thermal models. In the past it was not possible to use these models to calculate hadronic ratios in a new energy domain. In Table III we list predictions of the model for a beam energy of 40*A* GeV and compare them to experimental results obtained at CERN using Pb-Pb at 158*A* GeV. The main deviation can be found in ratios involving antibaryons. This is because the baryon chemical potential is predicted to be substantially larger at 40 GeV than at 158 GeV; this suppresses all antibaryons by an order of magnitude.

## VI. SUMMARY

We have shown that all results obtained in relativistic heavy ion collisions for beam energies between 1*A* GeV and 200*A* GeV can be summarized in a very simple way: when the average energy per hadron drops below 1 GeV, chemical freeze-out happens, the particle composition of the final state is fixed, and inelastic collisions cease to be important. This happens for Ni-Ni collisions at 1*A* GeV, for Pb-Pb collisions at 158*A* GeV and for S-S collisions at 200*A* GeV. It is thus independent of the beam energy, of the beam particle and by implication, of the size of the hadronic volume. Particle ratios for a beam energy of 40*A* GeV have been given in Table III. We consider these predictions as highly reliable.

The next stage of the evolution of the hadronic system is thermal freeze-out. Here the elastic collisions cease and the momenta of the final state particles are fixed. We have indicated that all available results are consistent with the fact that this happens when the energy density drops below 45 MeV/fm$^3$ or when the particle density is less then 0.05/fm$^3$. It is not possible yet to distinguish between these two possibilities with the presently available data.

## ACKNOWLEDGMENTS

We acknowledge stimulating discussions with P. Braun-Munzinger, B. Friman, M. Gaździcki, U. Heinz, W. Nörenberg, H. Oeschler, H. Satz, and J. Stachel.

[1] For a review see, e.g., U. Heinz, J. Phys. G **25**, 263 (1999); nucl-th/9907060.
[2] P. Braun-Munzinger, J. Stachel, J. P. Wessels, and N. Xu, Phys. Lett. B **365**, 1 (1995).
[3] P. Braun-Munzinger and J. Stachel, Nucl. Phys. **A638**, 3c (1998).
[4] P. Braun-Munzinger, I. Heppe, and J. Stachel, nucl-th/9903010.
[5] J. Letessier and J. Rafelski, J. Phys. G **25**, 295 (1999).
[6] C. Spieles, H. Stöcker, and C. Greiner, Z. Phys. C **74**, 319 (1998).
[7] F. Becattini, M. Gaździcki, and J. Sollfrank, Eur. Phys. J. C **5**, 143 (1998).
[8] I. G. Bearden *et al.*, Nucl. Phys. **A638**, 419c (1998).
[9] G. D. Yen, and M. I. Gorenstein, nucl-th/9808012.
[10] P. Braun-Munzinger, J. Stachel, J. P. Wessels, and N. Xu, Phys. Lett. B **344**, 43 (1995).
[11] J. Cleymans, D. Elliott, R. L. Thews, and H. Satz, Z. Phys. C **74**, 319 (1997).
[12] A. D. Panagiotou, G. Mavromanolakis, and J. Tzoulis, Phys. Rev. C **53**, 1353 (1996).
[13] J. Letessier, J. Rafelski, and A. Tounsi, Phys. Lett. B **328**, 499 (1994).
[14] J. Cleymans, D. Elliott, A. Keränen, and E. Suhonen, Phys. Rev. C **57**, 3319 (1998).
[15] J. Cleymans, H. Oeschler, and K. Redlich, nucl-th/9809031; Phys. Rev. C **59**, 1663 (1999).
[16] J. Sollfrank, J. Phys. G **23**, 1903 (1997), and references therein.
[17] F. Cooper and G. Frye, Phys. Rev. D **10**, 186 (1974).
[18] J. D. Bjorken, Phys. Rev. D **27**, 140 (1983).
[19] H. Appelshäuser *et al.*, NA49 Collaboration, Nucl. Phys. **A638**, 91c (1998); Eur. Phys. J. C **2**, 661 (1998).
[20] S. Chapman and J. R. Nix, Phys. Rev. C **54**, 866 (1996); J. R. Nix, *ibid.* **58**, 2303 (1998).
[21] J. R. Nix *et al.*, nucl-th/9801045.
[22] M. M. Aggarwal *et al.*, Phys. Rev. Lett. **83**, 926 (1999).
[23] I. G. Bearden *et al.*, Phys. Rev. Lett. **78**, 2080 (1998).
[24] E. Schnedermann, J. Sollfrank, and U. Heinz, Phys. Rev. C **48**, 2462 (1993).
[25] J. Alam, J. Cleymans, K. Redlich, and H. Satz, nucl-th/9707042.
[26] E. V. Shuryak, Nucl. Phys. **A638**, 207c (1998).
[27] B. Kämpfer, J. Phys. G **23**, 2001 (1997); hep-ph/9612336.
[28] Particle Data Group, C. Caso *et al.*, Eur. Phys. J. C **3**, 1 (1998).
[29] See, e.g., D. H. Rischke, in *Hadrons in Dense Matter and Hadrosynthesis*, edited by J. Cleymans, H. B. Geyer, and F. G. Scholtz (Springer, Berlin, 1999), pp. 21–70.
[30] D. H. Rischke (private communication).
[31] P. V. Ruuskanen, *Quark-Gluon Plasma*, edited by R. C. Hwa (World Scientific, Singapore, 1992), p. 519.
[32] J. P. Blaizot and J.-Y. Ollitrault, in *Quark-Gluon Plasma* [31], p. 393.
[33] J. Sollfrank and U. Heinz, in *Quark-Gluon Plasma*, edited by R. C. Hwa (World Scientific, Singapore, 1995), Vol. 2.
[34] R. Hagedorn and K. Redlich, Z. Phys. C **27**, 541 (1985).
[35] K. Zalewski, Acta Phys. Pol. **28**, 933 (1965); E. M. Ilgenfritz and J. Kripfganz, Nucl. Phys. **B62**, 141 (1973).
[36] J. Rafelski and M. Danos, Phys. Lett. **97B**, 279 (1980).
[37] K. Redlich and L. Turko, Z. Phys. C **5**, 201 (1980); L. Turko, Phys. Lett. **104B**, 361 (1981).
[38] B. Müller, *The Physics of the Quark-Gluon Plasma*, Lecture Notes in Physics 225 (Springer-Verlag, Berlin, 1985), pp. 91–104.
[39] C. Derreth, W. Greiner, H.-Th. Elze, and J. Rafelski, Phys. Rev. C **31**, 360 (1985).
[40] M. Gorenstein, V. K. Petrov, and G. M. Zinovjev, Phys. Lett. **106B**, 327 (1981).
[41] J. Cleymans, K. Redlich, and E. Suhonen, Z. Phys. C **51**, 137 (1991).
[42] F. Becattini, Z. Phys. C **69**, 485 (1996); F. Becattini and U. Heinz, *ibid.* **76**, 269 (1997).
[43] E. Andersen *et al.*, Phys. Lett. B **433**, 209 (1998).
[44] J. Cleymans and K. Redlich, Phys. Rev. Lett. **81**, 5284 (1998).
[45] M. Gaździcki, Z. Phys. C **66**, 659 (1995).
[46] M. Gaäzdzicki and D. Röhrich, Z. Phys. C **65**, 215 (1995).
[47] E. Laermann, Nucl. Phys. **A610**, 1c (1996).
[48] J. Rafelski, J. Letessier, and A. Tounsi, Acta Phys. Pol. B **27**, 1037 (1996).
[49] F. Becattini, J. Sollfrank, K. Redlich, and H. Satz, Nucl. Phys. **A638**, 399c (1998).
[50] M. Gaždzicki and M. Gorenstein, nucl-th/9803462.
[51] M. N. Asprouli and A. D. Panagiotou, Phys. Rev. C **51**, 1444 (1995); Phys. Rev. D **51**, 1086 (1995).
[52] H. Dobler, J. Sollfrank, and U. Heinz, Phys. Lett. B **457**, 353 (1999).
[53] B. Tomášik, U. A. Wiedemann, and U. Heinz, nucl-th/9907096.
[54] L. Ahle *et al.*, E866 and E917 Collaboration, Nucl. Phys. **A638**, 57c (1998).
[55] F. Wang *et al.*, NA49 Collaboration, hep-ph/9812218.
[56] F. Becattini, J. Phys. G **25**, 287 (1999).